On Axial Coherence of Interfacial Waves in Countercurrent Flow

M. Vijayan, S. Jayanti, and A. R. Balakrishnan
Dept. of Chemical Engineering, IIT-Madras, Chennai 600 036, India

DOI 10.1002/aic.10471
Published online May 16, 2005 in Wiley InterScience (www.interscience.wiley.com).

Keywords: gas-liquid flow, countercurrent flow, flooding, interfacial waves

Introduction

Flooding is the limiting condition of stable countercurrent gas-liquid flow in columns and has been the subject of extensive research over a number of decades. An exhaustive review of the subject, as pertaining to unpacked columns, has been given by Bankoff and Lee.[1] While a number of correlations exist in the literature to predict the onset of flooding, the topic of the mechanism of flooding has been debated and discussed widely in the recent literature. Briefly, there are two schools of thought on the flooding mechanism: (1) the formation and upward transport of large waves from the bottom of the column near the gas injection/liquid withdrawal point, and (2) the destabilization of the liquid film near the liquid inlet resulting in the formation of large waves. Direct visual evidence of formation of large waves at the liquid exit under flooding conditions has been reported by a number of researchers.[2,3,4] However, this idea was opposed by Zabaras and Dukler.[5] They measured the local instantaneous wall shear stress using an electrochemical method just below the liquid feed, as well as just above the liquid withdrawal point. They found that in all instances of countercurrent flow, including conditions along the flooding curve, the time-averaged wall shear stress was directed upward indicating that the velocity near the wall was downward. They also measured the instantaneous film thickness from two conductance probes located 0.053 m apart. Cross-correlation of these signals showed a well-defined peak at a measurable time delay even under flooding conditions. Zabaras and Dukler, therefore, concluded that waves were travelling downward even under flooding conditions and that they did not reverse direction at the flooding point. They explained the photographic observation of upward-travelling waves by McQuillan et al.[3] as a transient phenomenon generated by the small depressurization used by McQuillan et al. to induce flooding. Thus, Zabaras and Dukler argued that the process of flooding was controlled by conditions that existed at the or just below the feed rather than at the liquid exit.

Jayanti et al.[6] attributed the existence of different mechanisms of flooding to the effect of tube diameter. In small diameter tubes, a coherent, ring-like wave could be formed around the inside wall of the tube which could then be transported upward by the gas. A flooding model, based on the formation of a large standing wave at the flooding point was developed by Shearer and Davidson.[7] Jayanti et al. argued that such a wave would be very unstable in large diameter tubes and, hence, could not travel upward for long distances. Vijayan et al.[8] conducted flooding experiments in tubes of 25, 67 and 99 mm inner dia. and confirmed visually the existence of upward travelling waves in the 25 mm dia. tube under flooding conditions. In the larger diameter tubes, the waves were observed to move only a short distance before collapsing. Similar behavior was also observed by Biage et al.[9] in a duct of rectangular cross-section and by Watson and Hewitt[10] in a tube of 82 mm internal dia.

While there is, thus, a convergent view on the flooding mechanism, the careful experimental results of Zabaras and Dukler[5] remain unexplained. Specifically, their observations that the wall shear stress always indicated a downward moving flow and that the film thickness measurements recorded no upward-moving waves need to be explained in a manner consistent with the recent visual observations of flooding mechanisms. Toward this end, film thickness measurements have been conducted under conditions in which different flooding mechanisms prevailed. The details of these studies and the results obtained are reported here.

Details of Experimental Setup and Procedure

The experimental setup used in this study is similar to that used by Vijayan et al.[8] and Maharudrayya and Jayanti.[11] It consisted of two 4 m-long transparent acrylic columns of

Correspondence concerning this article should be addressed to S. Jayanti at sjayanti@iitm.ac.in.

internal dia. of 25 and 67 mm with common connections to air and water sources. In each case, air from a compressor entered test at the bottom. Water was fed at a height of 3 m from the bottom and was removed at a height of 1 m from the bottom. Thus, air passed through a one meter-long straight section before it encountered water flow. The injection and withdrawal of water were carried out smoothly using filter assemblies. Each filter assembly consisted of three elements: a stainless steel mesh that provided a large resistance to flow; a perforated cylinder that provided rigidity to the mesh; and an outer cylinder that housed the two and was connected to the pump through a valve. The stainless steel mesh was made up of an inner layer of 25 μm mesh sandwiched between two outer layers of 100 μm mesh size. This combination mesh was wrapped tightly and tack-welded on to the inside surface of a perforated cylinder which had an inner diameter slightly greater than that of the test section. The pressure in the outer cylinder of the feed assembly was maintained slightly higher than that in the test section to allow smooth entry of water into the test section. Similarly, the test section itself was maintained at slightly above atmospheric pressure (up to a maximum of 0.5 bar for the highest flow rates) in order to facilitate smooth withdrawal of water from the water outlet filter assembly. This, coupled with the one metre-long sections above and below the countercurrent flow part of the test section (Figure 1) enabled smooth entry and exit for both the phases.

The instrumentation consisted of an orifice meter for the measurement of input air flow rate; a bank of rotameters for the measurement of input water flow rate; a range of manometers for the measurement of pressure drop; and a set of pressure gauges to monitor the pressure in the test section. In addition to these steady-state measurements, the local, instantaneous film thickness was measured using pin-type conductance probes. The electrodes were made of a stainless steel rod of 2 mm dia. and were separated by an angular displacement of between 10 and 30° depending on the test section. Two sets of such conductance probes, separated by an axial distance of 0.12 m, were used in the experiments to measure the axial coherence of interfacial waves. The probes were driven by a dedicated electronic driving unit operating at 10 kHz. The readings from each probe were recorded typically at 1,000 Hz for a period of 20 s. The readings of a conductance probe can be sensitive to changes in temperature, and the electrical conductance of the water. In order to minimize errors associated with these, care was taken to maintain a constant temperature (to within one degree Centigrade) during the experiment. Also, a known amount of sodium chloride was added to the water to maintain a constant electrical conductance. The probes were calibrated using plug inserts over the range of interest. These measures led to fairly reproducible measurements of the film thickness. Results obtained for the mean film thickness under falling film flow conditions agreed very well with established correlations for laminar and turbulent flows[1] over a range of film Reynolds numbers.

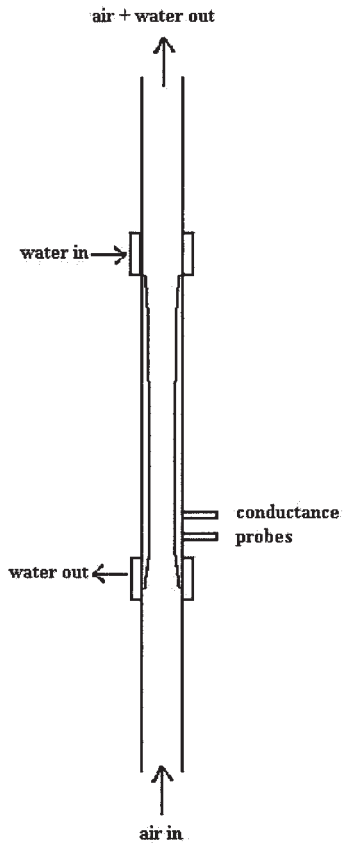

Figure 1. Experimental setup.

Results

The above experimental setup has been used to measure the film thickness for a range of air and water flow rates through each test section. The range of flow conditions included pre- and post-flooding conditions. In each run, the water flow rate was set at a specified level and the air flow rate was increased in small increments. Once the required air flow rate was obtained, the flow was allowed to settle for a few minutes before the recording of the film thickness. In all cases, the film thickness was measured at a fixed height of 0.16 m from the top of the water withdrawal assembly, that is, at a distance of 1.84 m from the liquid feed inlet. Simultaneously, film thickness was measured using a second conductance probe 0.12 m above, that is, at a distance of 1.72 m from the water feed level. The output voltage from each probe was converted into film thickness using the appropriate calibration curve, and was then digitally filtered to remove the high frequency (defined here as frequency greater than 25 Hz) noise. The mean film thickness was obtained directly from the time series while the signals were normalized (that is, the mean value subtracted) for spectral analysis. Typical results obtained from the measurement of the instantaneous film thickness for a water flow rate of 0.014 kg/s and an air flow rate of 0.00053 kg/s are summarized in Figure 2. The variation of film thickness with time is shown in Figure 2a over a two-second period. Assuming steady conditions, this film thickness trace can be visualized as a snapshot of the surface texture. From this point of view, one can see that the interface is far from smooth and is covered by a number of wave-like deformations of a range of wave lengths. This is confirmed by the power spectrum of the normalized fluctuations shown in Figure 2b which indicates nonzero power for a range of frequencies with a dominant frequency is in the range to 4 to 5 Hz (which justifies characterizing frequency components $>$25 Hz as being noise). The normalized cross-correla-

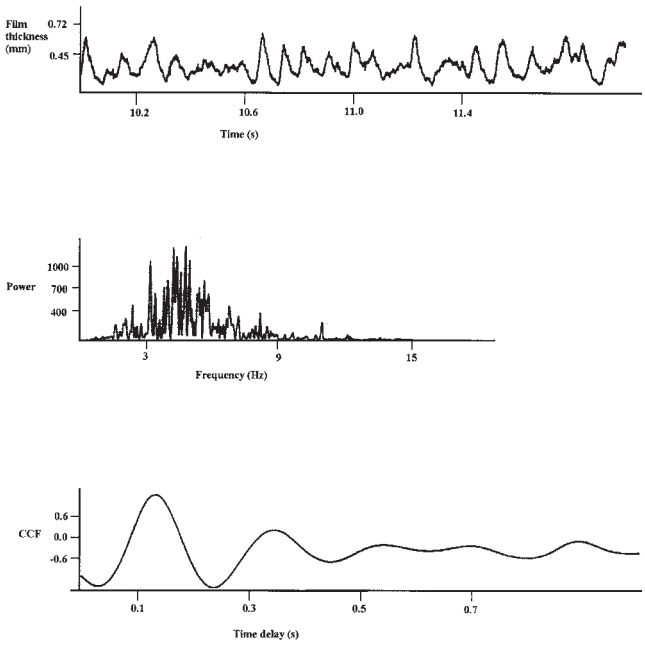

Figure 2. Results from the film thickness measurement and analysis: (a) variation of the film thickness over a 2-s period, (b) corresponding power spectrum of the film thickness fluctuations, and (c) cross-correlation function (CCF) of the fluctuations from two probes separated axially by 0.12 m.

tion function (CCF) between the film thickness variations from the two probes separated axially by 0.12 m is shown in Figure 2c. It exhibits a well-defined peak at a time delay of about 0.14 s, thus, giving a downward wave celerity (speed) of 0.86 m/s. The mean film thickness from the Nusselt theory[1] for this case is about 0.4 mm which is consistent with the variation shown in Figure 2a. The corresponding velocity of the interface is 0.78 m/s giving a ratio of the wave celerity to the surface velocity of about 1.10 for this case. This is in agreement with the experimental observation of Jones and Whitaker[12] that the wave celerity approaches the surface velocity as the film Reynolds number increases. It should be noted here that this measurements indicate the direction and speed of propagation of the dominant wave, but do not measure either the instantaneous or the time-averaged velocity profile within the liquid film.

Film thickness variation of the type shown in Figure 2 has been measured in tubes of 25 and 67 mm internal dia. for a range of flow conditions including pre- and post-flooding. Typical film thickness traces obtained at different air flow rates for a fixed water flow rate of 0.042 kg/s (corresponding to a liquid superficial Reynolds number of 2400) in the 25 mm dia. tube are shown in Figure 3. Here, the air flow rate is zero in Figure 3a and it corresponds to that of 80% of flooding air flow rate in Figure 3c, to flooding in Figure 3d and to post-flooding conditions in Figures 3e and 3f. The wave pattern is similar in Figures 3a and 3b, whereas significantly larger amplitude, low-frequency fluctuations are present in Figure 3d. These persist even after flooding (Figures 3e and 3f). These low frequency waves should therefore correspond to the frequency at which large upward-moving waves are repeatedly being created, as seen in visual observations.[8]

The corresponding plots of cross-correlation function between two probes axially separated by 0.12 m are shown in Figure 4. At low air flow rates (Figures 4a and b), there is a well-defined peak at a time delay of 0.95 s, which gives a downward velocity of 1.25 m/s. In Figure 4c, the peak is less clearly marked, although it is still there after roughly the same delay. Thus, the wave velocity does not change much right until the flooding point, as found experimentally.[5] However, the situation under flooding and post-flooding conditions is different from that found by Zabaras and Dukler. In this case, the axial coherence of the wave pattern is lost at and after flooding, although the film thickness traces show the presence of large amplitude waves. It was verified that there was no peak on the negative time delay axis (indicating an upward-moving wave) under these conditions. This should mean that these large waves are neither going up or going down steadily. Only a fraction of these large waves are carried up all the way beyond the liquid injection point while the rest collapse within a short distance. This would lead to the observed loss of axial coherence while not contradicting the upward transport of large waves as clearly observed in flow visualization studies.

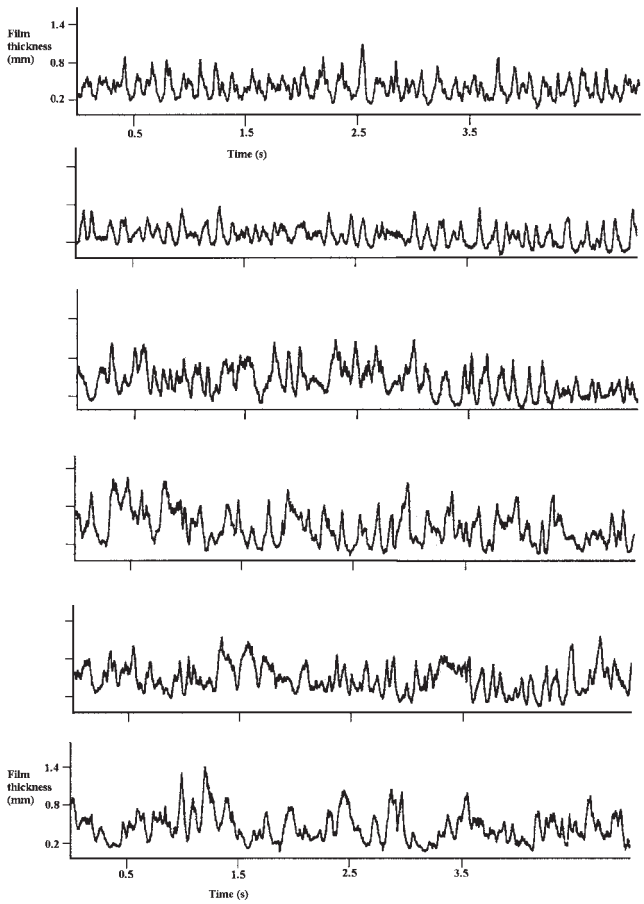

Figure 3. Film thickness traces obtained in the 25 mm dia. section at a water flow rate of 0.042 kg/s, and at air flow rates of (a) 0, (b) 0.00027, (c) 0.00060, (d) 0.00073, (e) 0.00100, and (f) 0.0020 kg/s.

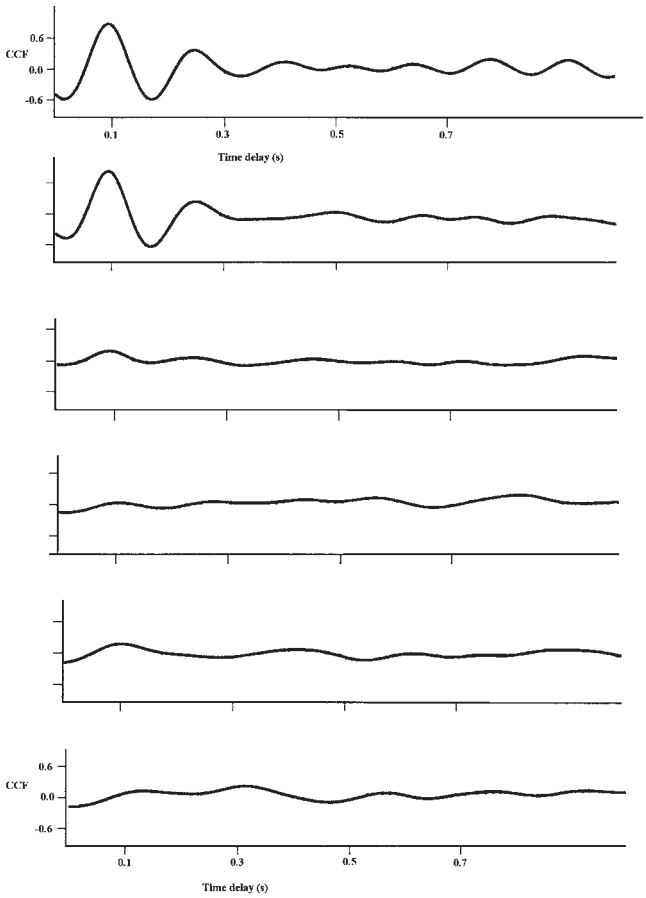

Figure 4. Cross-correlation function (CCF) between traces from two probes separated by an axial distance of 0.12 m for the flow conditions given in Figure 3.

A similar analysis has been carried out for the film thickness signals obtained from the 67 mm dia. test section. Typical variation of the cross-correlation function with air flow rate at a constant water flow rate of 0.111 kg/s (corresponding to a liquid superficial Reynolds number of 2400) is illustrated in Figure 5 for pre- and post-flooding conditions. Here, Figure 5a corresponds to the simple falling film case with no air flow rate while Figure 5d corresponds to the flooding condition. The significant aspect of the variation is that axial coherence is maintained (although somewhat reduced) even under flooding and post-flooding conditions (Figures 5d to f) unlike in the corresponding case of the 25 dia. tube. The time delay in the CCF plot is such that the waves are falling down even under flooding conditions. This is exactly the result that Zabaras and Dukler[5] obtained in their flooding experiments. Visual observations of Vijayan et al.[8] under these conditions show that there is a region of unstable film flow near the liquid inlet but that further down, essentially falling film type of conditions prevail. These film thickness measurements, which are taken about 1.6 m below the liquid inlet, confirm this by showing that the interfacial waves are travelling downward in this section.

The results shown in Figures 3 to 5 above are typical of the results obtained for the 25 and 67 mm dia. tubes. Similar results were obtained at other water flow rates. Measurements were also conducted for flooding in a tube of 99 mm inner dia. However, sufficient air flow rate was not available to achieve flooding for a range of water flow rates and flooding could be obtained only for a higher water flow rate of 0.444 kg/s (corresponding to a liquid Reynolds number of 6400). The cross-correlation functions at different air flow rates for this water flow rate are shown in Figure 6. Here, Figure 6e corresponds to the flooding condition, while Figure 6c corresponds to 90% of the flooding air flow rate. The variation of CCF, rather surprisingly, is unlike that of Figure 5 in that axial coherence is lost at the onset of flooding. Thus, it shows a behavior more typical of the small diameter tube and appears to contradict the supposed diameter effect on the flooding mechanism. However, this variation is consistent with the visual observations of flooding under these conditions. Vijayan et al.[8] reported a third mechanism, namely, carryover of droplets beyond the liquid injection point, which was found to prevail for large liquid flow rates in large diameter tubes. Under these conditions, the collapse of large interfacial waves gave rise to a large amount of droplet entrainment, part of which was carried away by the air stream resulting in a steady upward flow of liquid flow beyond the liquid injection point. While the major part of the falling film flow was regular, the liquid film

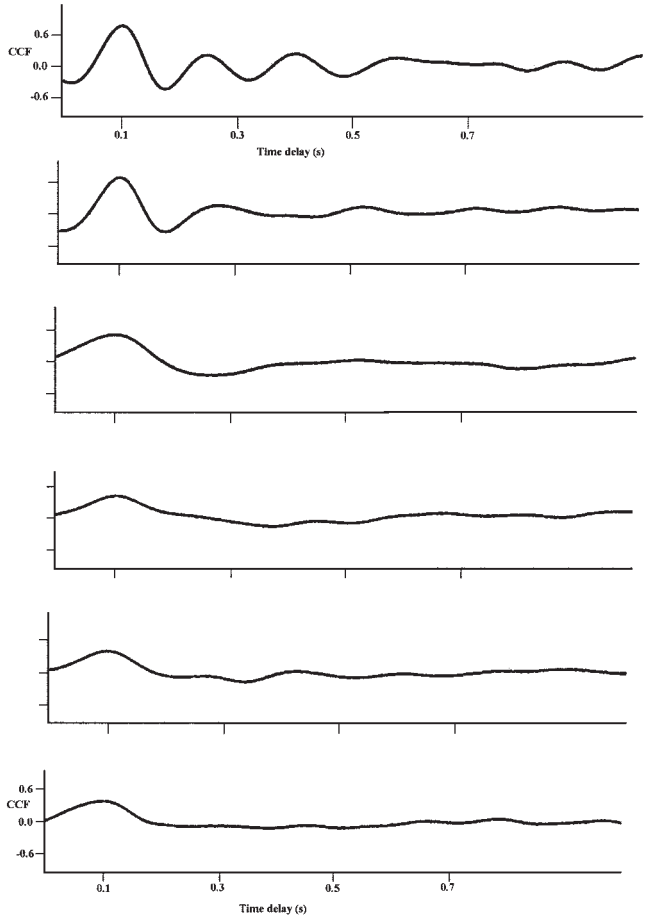

Figure 5. Cross-correlation function in the 67 mm dia. test section at a water flow rate of 0.111 kg/s, and at air flow rates of (a) 0, (b) 0.023, (c) 0.054, (d) 0.057, (e) 0.062, and (f) 0.065 kg/s.

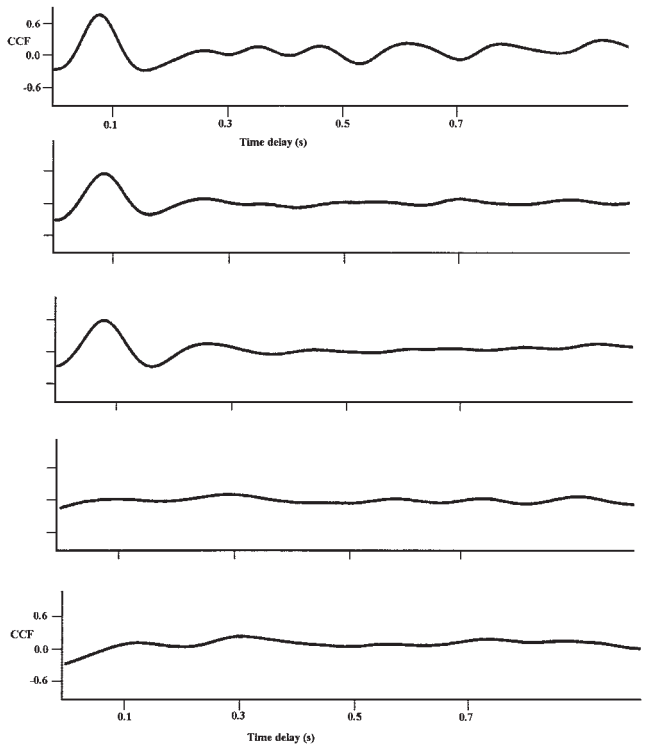

Figure 6. Cross-correlation function in the 99 mm dia. test section at a water flow rate of 0.444 kg/s, and at air flow rates of (a) 0, (b) 0.022, (c) 0.057, (d) 0.063, and (e) 0.064 kg/s.

flow near the liquid outlet was found to be chaotic due to the instability of the large interfacial waves. This resulted in the local loss of axial coherence for the interfacial waves under flooding conditions.

Discussion

The results presented earlier show that axial coherence of interfacial waves is a key indicator of the state of the liquid film under flooding conditions. In the absence of countercurrent flow of air, cross-correlation of film thickness traces from probes separated by a short axial distance shows a well-defined peak which can be associated with the time required for the dominant wave to traverse the separation distance. This axial coherence of interfacial waves is retained even when there is a countercurrent flow of air. Whether or not it is destroyed under flooding conditions depends on the flooding mechanism as well as on where the film thickness is measured. In small diameter tubes (or in conditions where flooding, that is, sustained liquid flow rate above the liquid injection point, is caused by repeated transport of waves from the bottom), axial coherence is lost due to some of the interfacial waves being carried upward repeatedly. In large diameter tubes, where interfacial waves cannot be carried upward over long distances, axial coherence may be retained even under flooding condition if the film thickness is measured sufficiently away from the chaotic, unstable zone, as illustrated in Figure 5. However, if measurements are made in the unstable zone, as for the data shown in Figure 6, then axial coherence is lost. Thus, film thickness measurements are a good indicator of the condition of the film flow, but not necessarily of the mechanism of flooding in the general case if measurements are restricted to a single location. Measurement of axial coherence at several points along the length may however indicate whether or not flooding has occurred.

Acknowledgments

The work reported here is supported by a research grant from the Department of Science and Technology, India.

Literature Cited

1. Bankoff SG, Lee SC. A critical review of the flooding literature. In: Hewitt GF, Delhaye JM, Zuber N. Multiphase science and technology. New York: Hemisphere Publishing, 1986: Chapter 2.
2. Suzuki KH, Ueda T. Behaviour of liquid films and flooding in countercurrent two-phase flow, part I: flow in circular tubes. *Int J Multiphase Flow*. 1977;3:517-532.
3. McQuillan KW, Whalley PB, Hewitt GF. Flooding in vertical two-phase flow. *Int J Multiphase Flow*.1985;11:741-760.
4. Govan AH, Hewitt GF, Richter HJ, Scott A. Flooding and churn flow in vertical pipes. *Int J Multiphase Flow.* 1991;17:27-44.
5. Zabaras GJ, Dukler AE. Countercurrent gas-liquid annular flow including the flooding state. *AIChE J.* 1988;34:389-396.
6. Jayanti S, Tokarz A, Hewitt GF. Theoretical investigation of the effect of diameter on flooding in gas-liquid flows. *Int J Multiphase Flow*. 1996;22:307-324.
7. Shearer CJ, Davidson JF. The investigation of a standing wave due to gas blowing upwards over a liquid film: its relation to flooding in wetted-wall columns. *J Fluid Mech*. 1965;22; 321-336.
8. Vijayan M, Jayanti S, Balakrishnan AR. Effect of tube diameter on flooding. *Int J Multiphase Flow*. 2001;27:797-816.
9. Biage M, Delhaye JM, Vernier P. The flooding transition: a detailed experimental investigation of the liquid film before the flooding point. ANS Proceedings, National *Heat Transfer Conf*. 1989:53-60.
10. Watson M, Hewitt GF. Effect of diameter on flooding initiation mechanism. Third International Conference on Multiphase Flow; June 8-12; 1998; Lyon, France.
11. Maharudrayya S, Jayanti S. Investigation of post-flooding conditions in countercurrent gas-liquid flow. *AIChE J*. 2002;48:212-220.
12. Jones LO, Whitaker S. An experimental study of falling liquid films. *AIChE J.* 1966;12:525-529.

Manuscript received Apr. 29, 2004, and revision received Nov. 25, 2004.